Computers & Geosciences 180 (2023) 105458

Contents lists available at ScienceDirect

Computers and Geosciences

journal homepage: www.elsevier.com/locate/cageo

ISTRICI – Tools for facilitating seismic depth imaging and velocity analysis with seismic unix

Umberta Tinivella *, Michela Giustiniani

National Institute of Oceanography and Applied Geophysics - OGS, Borgo Grotta Gigante 42C, 34010, Sgonico (TS), Italy

ARTICLE INFO

Keywords:
Seismic velocity
Pre-stack depth migration
Residual parameter
Common image gather
Open-source

ABSTRACT

ISTRICI was developed to facilitate the use of Seismic Unix, a free software designed to process seismic data. Seismic Unix is a powerful tool for performing pre-stack depth migration and using the residual parameters to update the seismic velocity model based on the pre-stack depth migration results. What is missing are codes and scripts that allow practical, interactive, and easy application of the Seismic Unix algorithms. Therefore, ISTRICI was developed to fill this gap. ISTRICI consists of three workflows (INTER, CIG and TRAD) for interactively performing residual velocity analysis and pre-stack depth migration, switching from one workflow to the next depending on the characteristics and type of seismic data. To demonstrate the flexibility and efficiency of our package, we describe the application of this tool on marine seismic data.

1. Introduction

Interpretation of seismic reflection data in complex geologic settings requires good seismic imaging, which is only possible if the velocity field is known with high accuracy. In this case, stacking velocities are not reliable because they are evaluated assuming flat horizons and constant lateral velocities at each common depth point (Yilmaz, 2001; Giustiniani et al., 2022). To avoid this problem, it is necessary to use a more accurate velocity analysis. For example, it is possible to use the residual moveout analysis, supposing a hyperbolic curve. The main limitation of a velocity estimation, using hyperbolic residual moveout, is related to the case of significant lateral variation; in fact, in this latter case, the residual moveout is not approximated by a hyperbola for large offset. So, the residual moveout corrections are evaluated considering only small offset. Consequently, the residual moveout velocity could be quite different from the root-mean square velocity (e.g., Yilmaz, 2001; Jones, 2010). Therefore, the velocity model building can be done only by using an iterative approach. Moreover, it is important to recall that in the case of complex geological settings, pre-stack depth migration (PSDM) is essential to obtain the correct depths and geometries of structures (Yilmaz, 2001).

In order to obtain an accurate geological velocity model, a robust velocity inversion method is required (see, for example, Jones, 2010, for a comprehensive overview of the approaches historically used in velocity model building). The velocity inversion is generally done in three stages: building an initial velocity model, performing an inversion with a selected algorithm, and updating the velocity model until the error criteria is less than a threshold (Yilmaz, 2001).

Reflection tomography is an essential approach for velocity analysis that handles lateral velocity variations. In the tomographic approach, applied to the inverse problem, the medium velocity is determined by minimising a misfit function that represents the deviation of traveltimes. The formulation in the tomographic approach is set up analytically, so some aspects of velocity inversion, such as stability, resolution and computational efficiency can be analysed (i.e., Jones, 2014). By using the tomographic approach, the velocity model can be discretized in three different ways: (1) layer-based model, (2) grid-based model, and (3) hybrid model (e.g., Jones, 2014; Sain and Nara, 2023). The layer-based model consists of layers characterised by lateral velocity variations and vertical variations from one layer to the next. In the grid-based model, the space is represented by pixels to which a velocity value is associated. In the hybrid model, the two previous concepts are combined; in fact, the model consists of interpreted layers, represented by regular or irregular pixels to which a velocity value is associated. So, the velocity varies laterally and vertically in each layer.

However, there are some difficulties in the tomographic approach. First of all, picking reflected events from seismic signals may prove difficult. For example, in the case of complex geological structures, the events in the unmigrated data are frequently distorted by correlated noise. Secondly, the raypath coverage could be sparse and, therefore,

* Corresponding author.
E-mail addresses: utinivella@ogs.it (U. Tinivella), mgiustiniani@ogs.it (M. Giustiniani).

https://doi.org/10.1016/j.cageo.2023.105458
Received 23 August 2022; Received in revised form 12 September 2023; Accepted 15 September 2023
Available online 16 September 2023

uniqueness is an issue, with multiple solutions being a possibility. Finally, the construction of raypaths is closely related to the position of the reflection, both in terms of depth and slope. Although the depth could be determined in an efficient way during the inversion procedure, the slope cannot be included as a parameter in the inverse problem; consequently, the slope is not determined with high accuracy (e.g., Jones, 2014).

PSDM provides a powerful tool for performing velocity analysis because of its high sensitivity to the velocity error and its ability to handle both reflector dips and lateral velocity variations (e.g., Yilmaz, 2001). In recent decades, thanks to the availability of high-performance computers, the iterative application of PSDM is the most commonly used method to determine the 2D and 3D seismic velocity fields (e.g., Loreto et al., 2007, 2012; Tinivella et al., 2009; Giustiniani et al., 2009; Vargas-Cordero et al., 2016, 2017, 2018 and references therein; Xiang and Landa, 2017; Guo and Schuster, 2017; Villar-Muñoz et al., 2018; 2019; He and Liu, 2020).

Two main approaches for migration velocity analysis have been developed: depth-focusing analysis (DFA) and residual curvature analysis (RCA). Details are reported, for example, in Yilmaz (2001). Here, we review the main characteristics of these two approaches.

Depth-focusing analysis is based on stacking power to measure velocity error. The DFA approach is based on these principles: (i) when the migration velocities are exact, the two imaging conditions, zero time and zero offset, yield a focused image during downward continuation; (ii) when the migration velocities are in error, reflected energy collapses to zero offset at depths that are inconsistent with the zero-time imaging condition; (iii) by interpreting the nonzero times at which focusing actually occurs, the migration velocities can be updated iteratively. The formula for updating velocity in the DFA approach is dip-limited, so repeated PSDM is required.

On the other hand, residual curvature analysis is based on using residual moveout to measure velocity error and in comparison to DFA approach, RCA is an alternative to migration velocity analysis that is able to overcome the dip limitations of DFA. In the RCA method, the migrated pre-stack data are sorted into common image gathers (CIGs). In each CIG, the migrated data have the same imaged horizontal location that is the principle in which RCA is based. After PSDM with an erroneous velocity, the depths of the reflections in a CIG from different offsets will differ from each other; the differences of reflection depth in CIGs provide information for updating the velocity iteratively.

Several algorithms are available to update the velocity model based on the difference between migration depth and focusing depth (DFA approach) or among imaged depth from different offsets (RCA approach). Liu and Bleistein (1995) proposed a robust iterative RCA approach to handle lateral velocity variations based on the perturbation method. The method is based on an analytical relationship between the residual moveout and residual velocity. The velocity is updated by computing a derivative function of depths of reflections with respect to velocity. Moreover, the raypath is determined by using the stationary-phase principle without requiring knowledge of the accurate reflector position. This theory is more accurate than conventional ones based on hyperbolic residual moveout in case of complex geological structures, for example when the medium has strong lateral velocity variations (Liu, 1995).

An open-source software package for seismic data analysis commonly used at academic level for performing PSDM is Seismic Unix (SU; Cohen and Stockwell, 2008). In particular, a very efficient algorithm for performing PSDM is available, based on the Kirchhoff algorithm and residual analysis of CIGs proposed by Liu and Bleistein (1995; see Appendix A). Based on the available algorithms in SU, we have developed a free package consisting of codes developed by us and SU codes to determine the seismic velocity field in different geologic settings. Here, we show the functionality of this free package, which we have named ISTRICI - Structural inversion of common image gathers.

2. Theory and methods

This section explains the key points for understanding our proposed ISTRICI package. For more details on SU, see Cohen and Stockwell (2008). Following the method of Liu and Bleistein (1995), the PSDM output consists of two migration sections characterised by the same phase, but different amplitudes. The algorithm performs the PSDM using the input and perturbed velocity models. The ratio of the amplitudes of these two PSDM sections is used to evaluate the residual velocity (i.e., Vargas-Cordero et al., 2010a). The result of the migration can be organized into CIGs: if the migrated reflections in the CIGs are flat, it means that a correct migration velocity was used to migrate the data (Yilmaz 2001). By contrast, the slope of the reflections in the CIGs indicates an error in the migration velocity, which can be corrected by analyzing the residual energy and then updating the velocity (code available in SU; Liu and Bleistein, 1995). The residual energy (called the r-parameter) is a measure of the flatness deviations of the reflections along the offset in each CIG (i.e., Tinivella et al., 2009). A zero value for the r-parameter means that the velocity is corrected at the corresponding reflection. If the r-parameter has a negative/positive value, it means that the velocity must be increased/decreased. Then, using the theory of Liu and Bleistein (1995), the r-parameter is converted to a residual velocity used to update the input velocity (Appendix A). It is important to remember that, when the medium has strong lateral velocity variations, the algorithm works adequately even with small velocity corrections. All steps, such as PSDM, CIG analysis, r-parameter evaluation, velocity update, are performed iteratively until all reflections in the CIGs are reasonably flat, i.e. when the variation of the depth of the reflector versus offset is sufficiently small in each CIG (see details in Appendix A and Vargas-Cordero et al., 2010a). Note that this approach provides both sensitivity and error estimations for migration-based velocity analysis, which is helpful in assessing the reliability of the estimated velocity (Appendix A).

The novelty of the ISTRICI package is to propose three different ways to organize the CIGs to improve the seismic velocity analysis depending on different elements, such as targets and characteristics of the data, optimizing the result quality and reducing the time needed to analyze the r-parameters in the residual semblances.

ISTRICI has been developed on the basis of the most common cases: (i) the continuity of some reflections along the seismic line, such as the seafloor, suggests that the picking procedure can be performed semi-automatically in the residual semblance; (ii) the availability of the interpretation of the seismic section suggests that the velocity analysis can be performed along the interpreted reflectors; (iii) in complex geological settings and/or in the presence of non-continuous reflectors, the velocity analysis can be performed as a function of depth rather than in a layer-stripping approach.

The user can choose and move from one workflow to another in order to better resolve the targets and/or scientific questions on the basis of the characteristics of the data. Moreover, for the same purposes, the user can update and modify the codes related to the velocity analysis.

STEP 1 of all workflows consists of performing PSDM obtaining two outputs: the standard migration and the additional migration with extra amplitude (see details in Liu and Bleistein, 1995). Before this step, an initial velocity model has to be created, which is input into the workflow along with the seismic data for STEP 1.

In the INTER workflow, the r-parameter analysis is performed along a selected reflector. The procedure of INTER consists of four steps, which are described in Fig. 1. First, after PSDM, the migrated section is interpreted by picking the selected reflector; then, the picks are interpolated to obtain one pick for each migrated trace (STEP 2). Then, in a selected range of CIGs, residual propagation analysis is calculated over the depth of the selected reflector with a defined window based on the wavelength of the reflection. The results are displayed in a table where the x-axis indicates the CIGs number and the y-axis indicates the r-parameter.

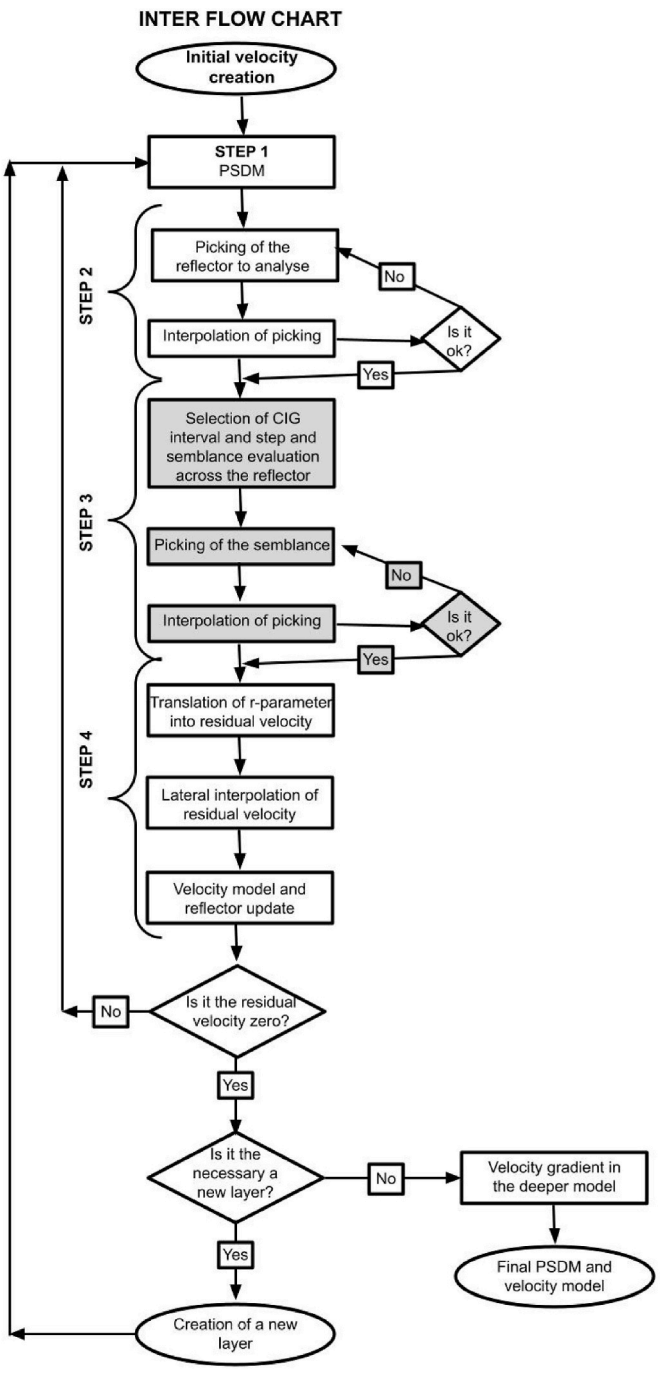

Fig. 1. Flowchart describing the INTER workflow.

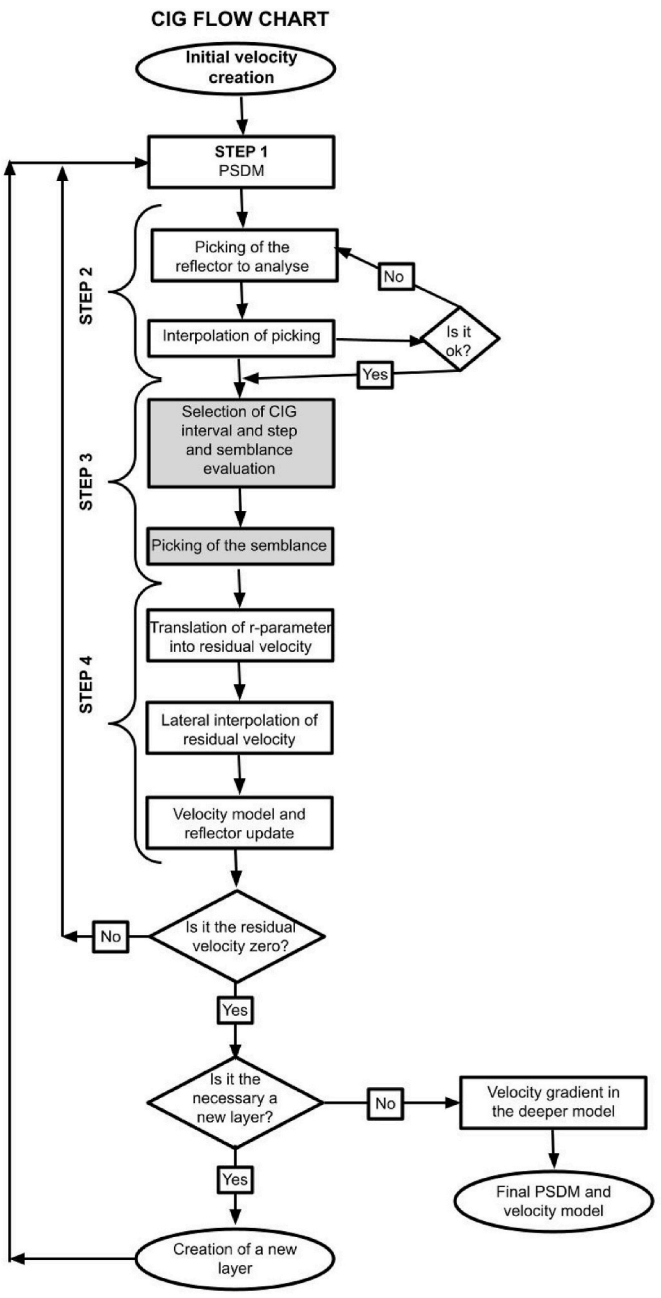

Fig. 2. Flowchart describing CIG workflow.

Then, the operator simply selects the r-parameter along the reflector; the selections are interpolated to obtain an r-parameter value for each CIG (STEP 3). STEP 4 consists of evaluating the velocity and updating the reflector depth for each CIG based on the r-parameter value and migration results. The procedure is repeated from STEP 1 to STEP 4 until the difference between two successive iterations is less than a certain threshold. The final velocity model is composed of the selected layers. In each layer, the velocity changes in horizontal direction, but is constant in depth.

In the CIG workflow, the analysis of the r-parameters is performed along a selected reflector, but unlike the INTER workflow, the picking is performed by analysing the total semblance at each selected CIG (see also Vargas-Cordero et al., 2010a). This workflow also requires four STEPS, as described in Fig. 2. In STEP 2, the migrated section is interpreted and the picking of a reflection is performed. As in the INTER workflow, the picks are interpolated along the seismic section. STEP 3 consists of picking the r-parameter at depth in proximity of the picked reflector at selected CIGs. To help the user, the code specifies the depth of the selected reflector at the semblance to pick the r-parameter where the energy is higher. In this way, the interpretation of the seismic line (i.e., the depth of the target interface) is changed according to the maximum coherence of the semblance. STEP 4 is the same as the one in the INTER workflow as well as the final result. Also in this case, STEPs 1-4 are repeated until the difference between successive iterations is less than a certain threshold.

The TRAD workflow is different from the other two workflows because STEP 2, dedicated to the interpretation of the migration section, is not required. In fact, only two STEPs are required in this workflow in addition to STEP 1 (Fig. 3). STEP 2 consists in selecting the maximum energies in the semblance at selected CIGs. Of course, the number of

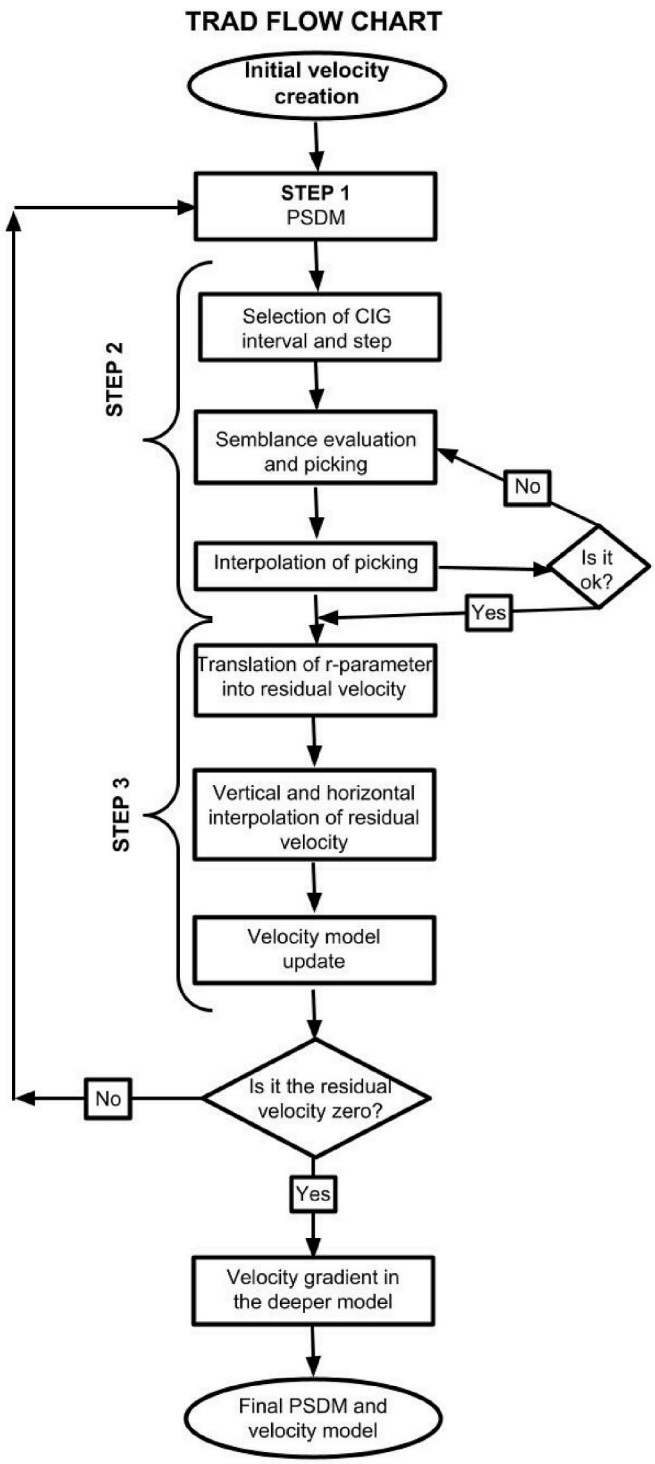

Fig. 3. Flowchart describing TRAD workflow.

measurements at each CIG may be variable based on semblance quality. STEP 3 is used to evaluate the residual velocity based on the selected r-parameter values and the two initial steps. The residual velocity is first interpolated over depth and then horizontally. The resulting residual velocity field is added to the input velocity model. Again, STEPs 1-3 are repeated until the r-parameter is approximately zero at all selected CIGs. Note that in the case of marine seismic data, it is possible to adopt the TRAD workflow after the water velocity layer has been established.

The final velocity model obtained by using TRAD is not organized in velocity layers; an additional tool of ISTRICI allows to build a velocity model in selected layers when an interpretation of the seismic line is provided. In this way, it is possible to switch from one workflow to another at each stage of the inversion.

Once the procedure is completed, ISTRICI can include a velocity gradient below the last inverted layer or a defined surface before performing the final PSDM to improve the seismic imaging.

Fig. 4 shows an example of the use and the integration among all workflows. The starting point is the constant velocity (panel 1). Then, by using the INTER workflow, the water velocity is determined (panel 2). After fixing the water velocity (panel 3), the velocity of the shallow structures is defined by using the CIG workflow (panel 4). Then, fixing the shallower velocity (panel 5), the velocity of the deeper part is defined by using the TRAD workflow (panel 6). Finally, a velocity gradient is included for the not-analysed deep layers on the basis of the far-offset value (panel 7).

3. Results

Here we present only an example of the results obtained with the INTER and TRAD workflows, whereas the results obtained with the application of the CIG workflow have already been published (i.e., Tinivella et al., 2009; Loreto et al., 2011; Vargas-Cordero et al., 2010b). The seismic dataset presented here was acquired offshore the Antarctic Peninsula in order to characterise the gas hydrate and free gas presence in marine sediments in the framework of the Italian Antarctic Program (PNRA). The data were acquired by using a 120-channel streamer with receiver and shot distance equal to 25 m; the near-offset was equal to 150 m and the sample rate was 2 ms (i.e., Loreto et al., 2011). The procedure used to obtain this example is based on Fig. 5; the CIG workflow is not considered here because it is extensively used and explained in literature as aforementioned (i.e., Vargas-Cordero et al., 2021 and references therein).

Before performing PSDM, some processing steps were applied, such as geometry insertion, as already well-described in the literature (e.g., Giustiniani et al., 2018; Tinivella et al., 2009). For marine data, we propose to use the INTER workflow to define and fix the seawater velocity, since the seafloor reflection is strong and continuous along the whole seismic line. An initial velocity field is required to perform PSDM. The propagation velocity of seawater is generally about 1500 m/s; therefore, we used this velocity to build the initial velocity model. The size of the 2D output grid was 25 m in depth, which is approximately the wavelength, and 50 m in the horizontal direction, which is twice the shot and receiver distances. The horizontal length of the grid was 46,000 m, while it was 5000 m in the vertical direction. Thus, the grid consisted of 921 cells in the horizontal direction and 201 in the depth direction. In order to reduce the time required to perform the PSDM, a high-performance computer was used.

After performing the first PSDM by using an initial constant velocity model of 1500 m/s, the seafloor reflector was picked. As explained earlier, the obtained picks were interpolated to obtain a seafloor depth for each CIG. Along the picked seafloor depth, a semblance was calculated considering a window over the seafloor reflector (Fig. 6); in this case, a window of $\pm$30 m was chosen based on the wavelet length of the seafloor reflector. We then selected a CIG every 100 m to determine the r-parameter along the seafloor reflector, taking into account the radius of the Fresnel zone and assuming that strong lateral velocity changes are not expected (e.g., Yilmaz, 2001). The picks were interpolated to obtain an r-parameter value for each CIG. The r-parameters were used to update (i) the velocity model and, after applying a new PSDM, (ii) the seafloor depth. This procedure (STEPs 2–4; see Fig. 1) was iteratively repeated about 20 times until the energy was well-focused around zero, as shown in Fig. 6. In Fig. 7, the comparison between the initial constant velocity field with the obtained migrated section and the final velocity field superimposed on the final migrated section is shown.

After defining and fixing the seawater velocity, we used the TRAD workflow to define the seismic velocity below the seafloor, adopting as

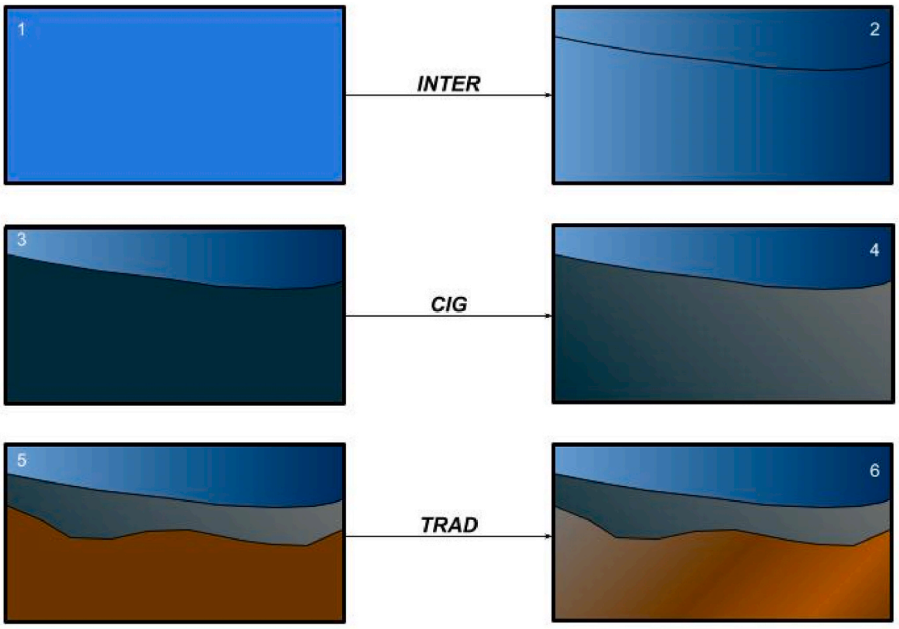

Fig. 4. Example of velocity update by using ISTRICI workflows. Panel 1: initial constant velocity. Panel 2: velocity and geometry of the shallowest layer after INTER analysis. Panel 3: initial velocity for CIG workflow in which the velocity and geometry of the shallowest layer are fixed. Panel 4: velocity and geometry of the second layer after CIG analysis. Panel 5: initial velocity for TRAD workflow in which the velocity and geometry of the shallower layers are fixed. Panel 6: velocity of the deeper part after TRAD analysis. Panel 7: velocity field of the last inverted layer with the introduction of the velocity gradient for the not-analysed deep layers.

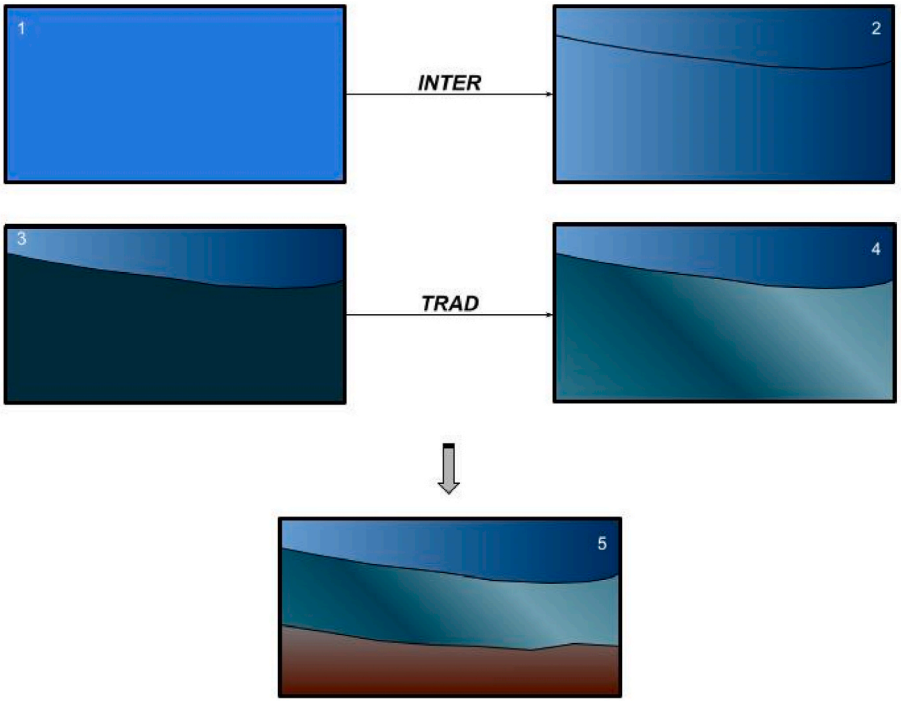

Fig. 5. Example of velocity update by using ISTRICI workflows. Panel 1: initial constant velocity. Panel 2: velocity and geometry of the shallowest layer after INTER analysis. Panel 3: initial velocity for TRAD workflow in which the velocity and geometry of the shallowest layer are fixed. Panel 4: velocity of the deeper part after TRAD analysis. Panel 5: velocity field of the last inverted layer with the introduction of the velocity gradient for not-analysed deep layers.

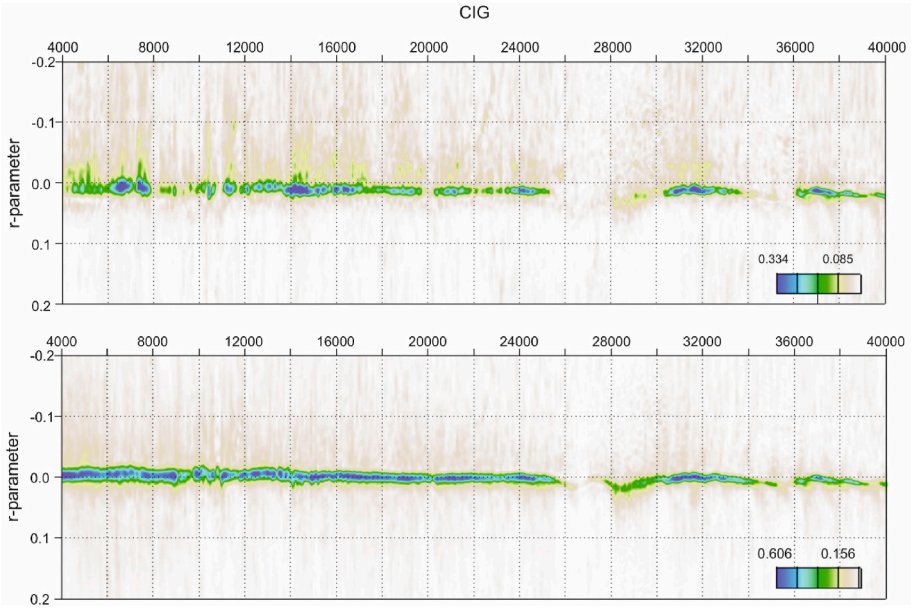

Fig. 6. Example of semblances used for residual velocity analysis with INTER workflow. The upper panel represents the semblance with an initial velocity of 1500 m/s, while the lower panel is the semblance with the final variable velocities along the seismic line.

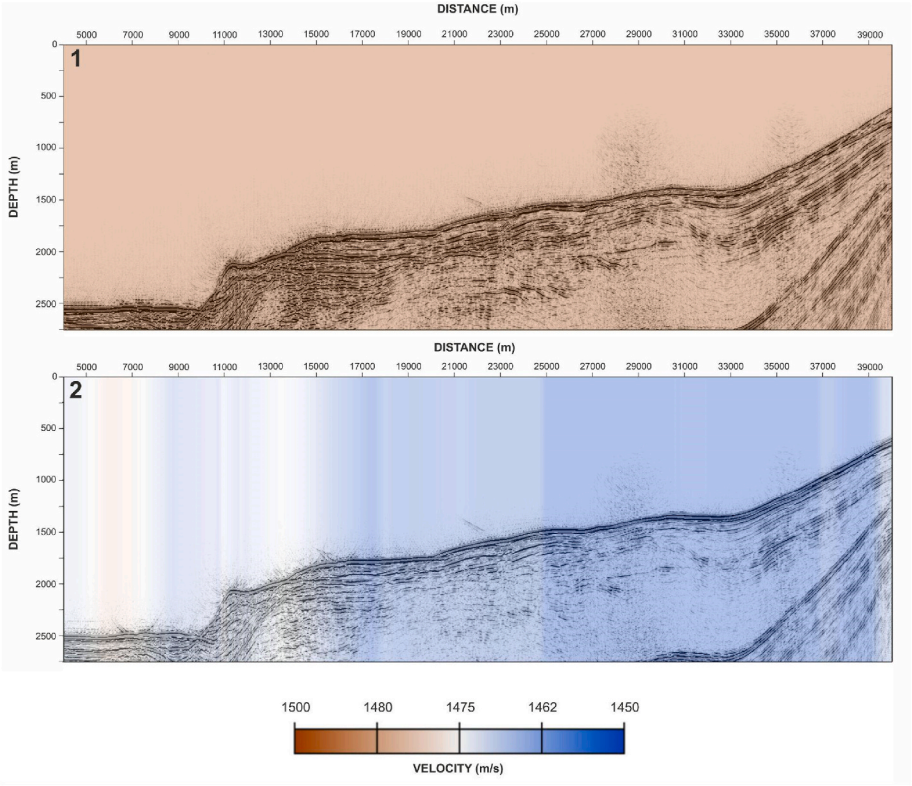

Fig. 7. Panel 1: initial velocity field (1500 m/s) superimposed on the migrated section obtained by using the initial velocity. Panel 2: final velocity field (obtained applying INTER workflow) superimposed on the final migrated section. Note that the higher initial velocity field with respect to the final one allows better highlighting the deeper reflectors which are characterised by higher velocities compared to the water column.

input velocity the final velocity field obtained by using INTER workflow with the same grid parameters. After PSDM, we performed the residual velocity analysis on the obtained CIGs (STEP 2; see Fig. 3) in three steps, increasing the horizontal resolution step by step. Fig. 8 shows an example of the semblance and CIGs panels used for the residual velocity analysis. On the semblance (upper panels), the maximum energy must be selected in accordance with the reflectors on the CIGs (lower panels). We performed the residual velocity analysis twelve times every 800 m for a total of 46 CIGs to define a regional trend of velocity distributions and identify critical areas. Then, we refined the residual velocity analysis considering a CIG step of 400 m for a total of 91 CIGs along the entire seismic line. In proximity of the boundary (0–4000 m and

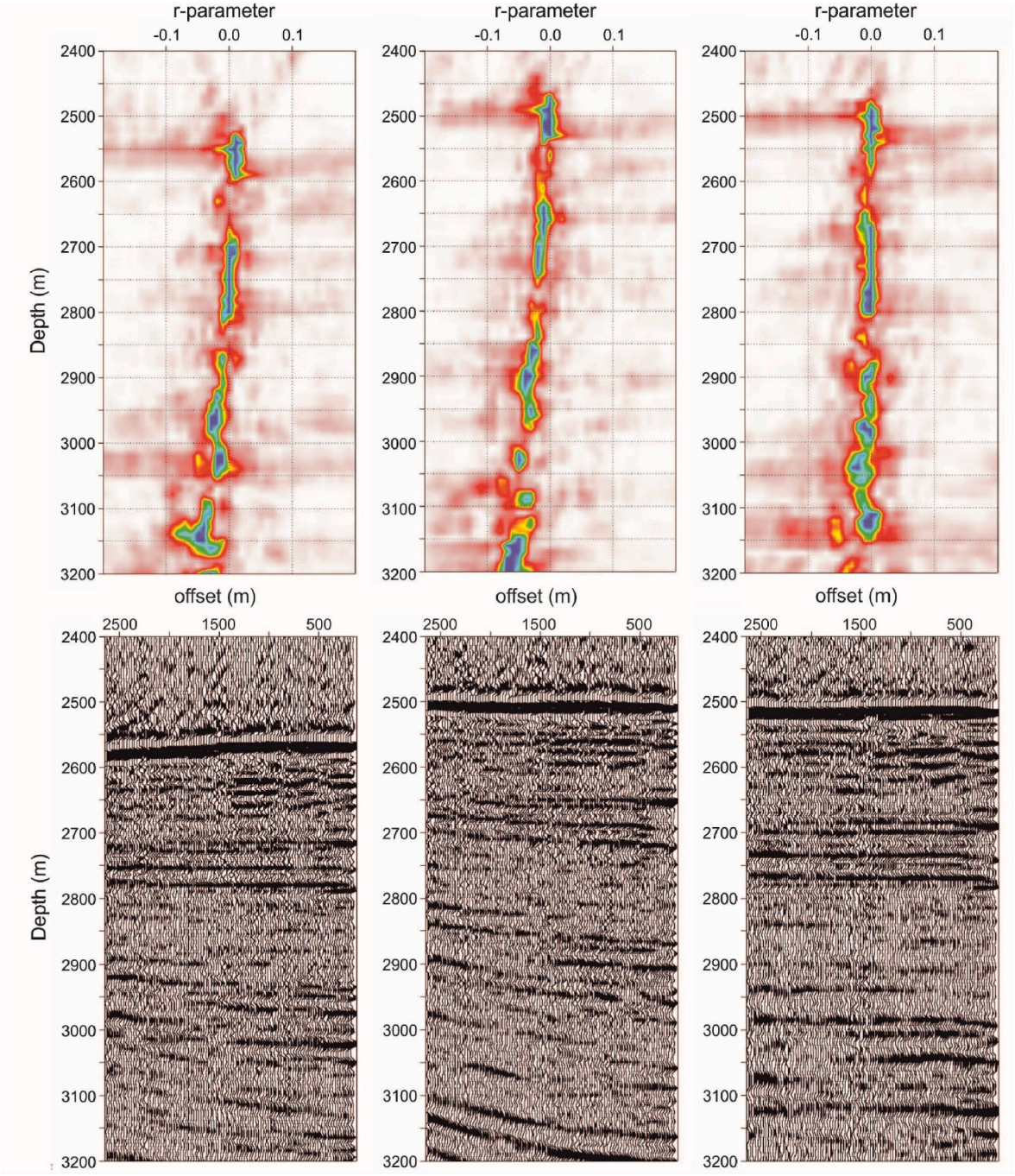

Fig. 8. Example of a CIG (bottom panel) with relative semblance (top panel) considering initial velocity (left panels), water velocity obtained with the INTER workflow (middle panels), and final velocity obtained with the TRAD workflow (right panels). The offset in the CIG indicates the distance between shot and receiver positions. See text for details.

40,000–46,000 m), where residual velocity analysis is not performed due to low seismic data coverage, the velocities obtained for the first and last CIG were assigned. After about 25 iterations, we defined the regional seismic velocity field; we then further refined the velocity model by performing a residual velocity analysis every 200 m for a total of 181 CIGs. To improve the velocity fields and increase the horizontal resolution, we focused on specific sections of the line where the r-parameter deviates significantly from zero; The TRAD workflow allows the velocity model to be analysed locally rather than interpolating across the entire seismic line. In the end, after about 10 iterations in each selected part, we smoothed the velocity field and added a velocity gradient of 0.4 s^{-1} for depths greater than 3000 m in order to perform the final PSDM (Fig. 9).

Before stacking the CIGs in order to obtain the final migrated section, some processing steps were applied to improve the imaging. For example, a filter was applied to emphasise the targets (the Bottom Simulating Reflector) and a mute of the larger offsets was applied to zero the noisiest part of the data. Then, the CIGs were stacked and visualised in Fig. 9.

4. Discussion and conclusions

The ISTRICI package consists of three workflows (INTER, CIG and TRAD) for interactively performing residual velocity analysis and PSDM

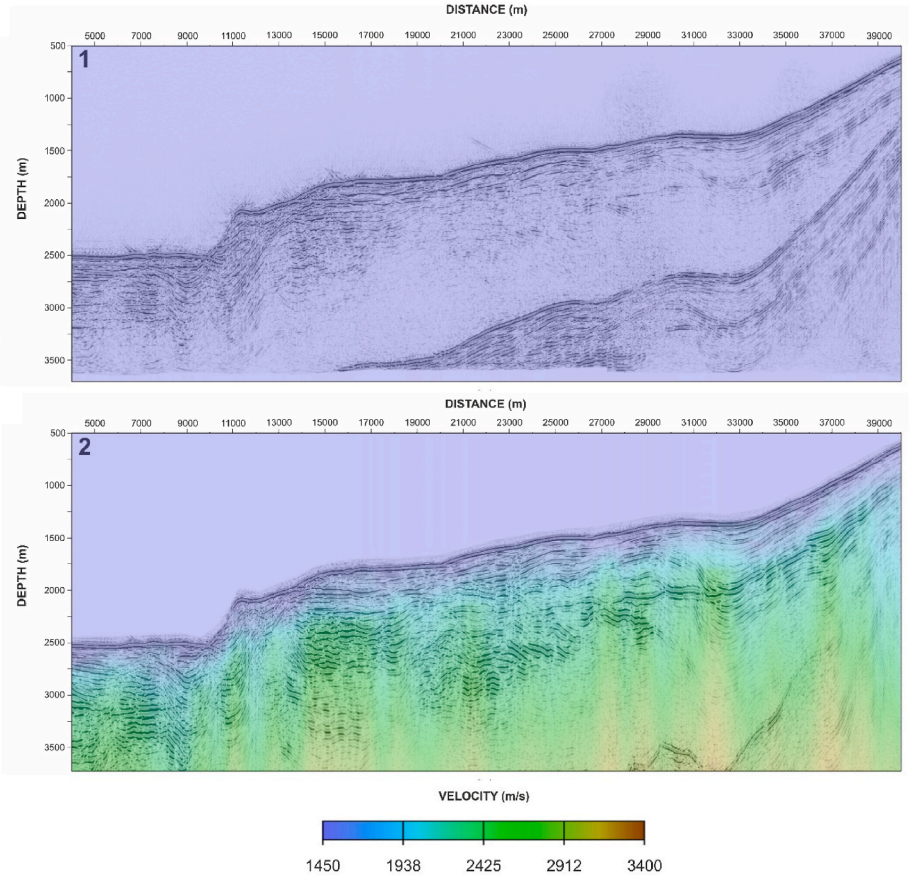

Fig. 9. Panel 1: velocity field (obtained applying INTER workflow) superimposed on the migrated section. Panel 2: final velocity field (obtained applying TRAD workflow) superimposed on the final migrated section. Note that a velocity gradient has been applied on not-analysed deep layers.

using codes developed by us integrated into SU, an open source processing package. SU is a powerful tool for performing PSDM and converting r-parameters into velocity corrections based on PSDM results. What was missing were codes and scripts that allow the use of SU algorithms in a practical, interactive and simple way to perform seismic velocity analysis in any type of seismic data. Therefore, ISTRICI was developed to fill this gap.

It is important to underline that ISTRICI proposes a philosophy to perform velocity analysis by iteratively using the PSDM. In fact, even if we propose the use of SU, because it is an open-source code, and Liu's approach, the user can change the algorithm and/or the codes to better solve their scientific problem. In fact, the user can change the codes in order to optimise the analysis of seismic data on the basis of the target and the characteristics of the data.

Liu's approach is based on the assumption that there is a linear relationship between the residual traveltime and the residual velocity if small velocity perturbations are considered. In the SU code, only one parameter is supposed in the linearization step. In any case, as shown in Appendix A, it is possible to consider many parameters, if necessary. Note that, if too many parameters are considered, the solution will be underdetermined and unstable. Consequently, it is essential to characterise the velocity distribution by choosing appropriate parameter numbers on the basis of the complexity of the target and seismic data characteristics.

Regarding the seismic data, the accuracy of velocity analysis for a CIG is best for large offsets and well-separated shot points, which is well-known (Yilmaz, 2001). Interestingly, it is also better for a reflector with positive dip (i.e., receiver of common shot images located in down-dip direction relative to the shot point; Liu, 1995).

The final velocity model depends on the signal/noise ratio in seismic data and the power of the stationary phase method. In fact, Liu's approach is robust only if the dominant seismic wavenumber is large compared to the length scale of the velocity variation.

Regarding the Kirchhoff PSDM algorithm, a smooth velocity is required for velocity estimates by perturbation. So, thin layers cannot be resolved with this approach. On the other hand, for extremely complex geological structures, such as the Marmousi model, it is very difficult to identify the correct velocity model, requiring powerful PSDM algorithms and advanced velocity analysis techniques. In this case, Liu's approach remains a useful tool for updating a velocity model if geological data is used as a constraint.

Within ISTRICI, velocity analysis can easily be performed by moving from one workflow to the other. For example, the velocity field shown in Fig. 9 was obtained by using the workflow INTER to define the velocity of the seawater (panel 1) and the TRAD workflow for the layers below the seafloor, with a detailed analysis of part of the seismic line (panel 2). Note that this tool is very effective, since it was developed for specific cases, such as the presence of a body with a velocity anomaly. Our codes were developed and improved after many tests that allowed identifying critical steps. As mentioned before, it is worth highlighting that the codes and scripts can easily be modified by the user if necessary. Finally, ISTRICI can be used in the present form for multichannel seismic data, ocean bottom seismometer data, ocean bottom cable data as well as land data.

As suggested by Liu (1995), this velocity analysis approach can be extended to the 3-D case, converted waves and anisotropic media. In the 3-D case, the eq. A.6 in Appendix A can be rewritten considering the vector that denotes the reflection point as a 3-D vector, just as the parameter that represents the half-offset will become a 2-D vector. In the case of converted waves, the perturbation parameter is related to the

shear wave velocity. For anisotropic media, more parameters are necessary to describe velocity distribution. So, Liu's approach provides a basis for developing computational techniques of velocity analysis in all types of seismic data and media.

Computer code availability

ISTRICI can be downloaded from the following public repository: https://github.com/utinivella/ISTRICI; a README file is provided for each workflow (INTER, CIG, and TRAD); an example is also available. ISTRICI uses codes from Seismic Unix, free software that can be downloaded here: https://wiki.seismic-unix.org/doku.php.

Authorship statement

U. Tinivella proposed the methods and programmed the software. M. Giustiniani participated in the software testing and suggested the updating of the codes. All authors contributed to the writing and the revision of the manuscript.

Declaration of competing interest

The authors declare that they are not aware of any competing financial interests or personal relationships that could have influenced the work in this publication.

Data availability

Data will be made available on request.

Acknowledgements

This study was supported by the Italian Ministry of Education, Universities and Research in part under the extraordinary contribution for Italian participation in activities related to the international infrastructure PRACE-The Partnership for Advanced Computing in Europe (www.prace-ri.eu; Decreto MIUR No. 631 of August 8, 2016) and in part by the PRIN Project entitled: "Methane recovery and carbon dioxide disposal in natural gas hydrate reservoirs". We are very grateful to Ivan Vargas-Cordero for useful discussions. The seismic data was acquired in Antarctica with the support of the Programma Nazionale di Ricerche in Antartide (PNRA). We thank the anonymous reviewers for their useful comments that helped significantly improve the manuscript.

Appendix A

In this Appendix, we report the theory described in Liu and Bleistein (1995) to build the velocity model by iteratively using the PSDM. Hereafter, we named it Liu's approach for simplicity.

Velocity analysis by perturbation

Liu's approach is based on the assumption that there is a linear relationship between the residual traveltime and the residual velocity if small velocity perturbations are considered. Moreover, the raypath is determined by using the stationary-phase principle and the imaging equations are used.

Let us consider the 2-D common offset case. The following imaging equations display a general relationship between the imaged depth and migration velocity:

$$\tau_s(x_s, x) + \tau_r(x, x_r) = t(y, h) \tag{A.1}$$

$$\frac{\partial \tau_s}{\partial y} + \frac{\partial \tau_r}{\partial y} = \frac{\partial t}{\partial y} \tag{A.2}$$

where x is a 2-D vector that denotes the reflection point, x_s and x_r are the source and reflection point position, respectively. τ_s is the traveltime for a downgoing wave from x_s to x and τ_r is the traveltime for an upgoing wave from x to x_r. y denotes the midpoint and h the half-offset. At a CIG, the imaged depth z can be determined as a function of h. If the migration velocity is equal to the true velocity, z will be independent of h; otherwise, z varies with h and provides information on velocity distribution.

Eq.s A.1 and A.2 are not linear, but can be linearised by using a perturbation. Suppose that the velocity distribution v is characterised by a parameter or a family of parameters λ:

$$v = v(x; \lambda) \tag{A.3}$$

So, the problem of velocity estimation becomes parameter estimation. For simplicity, let us assume that λ is a single parameter. Differentiating eq. A.1 with respect to λ and by using eq. A.2, we obtain:

$$\left[\frac{\partial \tau_s}{\partial z} + \frac{\partial \tau_r}{\partial z}\right] \frac{\partial z}{\partial \lambda} = -\frac{\partial \tau_s}{\partial \lambda} - \frac{\partial \tau_r}{\partial \lambda} \tag{A.4}$$

Let θ_s or θ_r be the angle between the raypath from the source or the receiver, respectively, and the vertical at x. By using eq. (A.4), the derivative of z with respect to λ is:

$$\frac{\partial z}{\partial \lambda} = g(x, h) \tag{A.5}$$

where

$$g(x,h) = -\left[\frac{\partial \tau_s}{\partial \lambda} + \frac{\partial \tau_r}{\partial \lambda}\right] \frac{v(x;\lambda)}{cos\,\theta_s + cos\,\theta_r} \quad \text{A.6}$$

The derivative function g represents, therefore, the relationship between z and the migration velocity.

Let us assume the true parameter λ^* and the true reflection depth z^*. Let us assume a small perturbation:

$$\delta\lambda = \lambda^* - \lambda \quad \text{A.7}$$

Then, z will have a perturbation equal to:

$$\delta z = z^* - z(x,h) \approx \frac{\partial z}{\partial \lambda}\delta\lambda \quad \text{A.8}$$

Finally, by using eq. A.5, we obtain:

$$\delta z = g(x,h)\ \delta\lambda \quad \text{A.9}$$

Eq. (A.9) is valid for any velocity distribution, reflector dip and offset if the velocity perturbation is sufficiently small.

When the velocity distribution is characterised by multiple parameters $\widehat{\lambda} = (\lambda_1, \lambda_2, ..., \lambda_n)$, δz will depend on the perturbation of all these parameters and the eq. A.9 becomes:

$$\delta z(x,h) = \sum_{i=1}^{n} \frac{\partial z}{\partial \lambda_i} = \sum_{i=1}^{n} g_i(x,h)\delta\lambda_i \quad \text{A.10}$$

where

$$g(x,h) = -\left[\frac{\partial \tau_s}{\partial \lambda_i} + \frac{\partial \tau_r}{\partial \lambda_i}\right] \frac{v(x;\widehat{\lambda})}{cos\,\theta_s + cos\,\theta_r} \quad \text{A.11}$$

The true parameter can be estimated by:

$$\widehat{\lambda} * = \widehat{\lambda} + \delta\widehat{\lambda} \quad \text{A.12}$$

and the true depth can be approximated as follows:

$$z^* \approx z(x,h) + \delta z(x,h) = z(x,h) + \sum_{i=1}^{n} g_i(x,h)\delta\lambda_i \quad \text{A.13}$$

The true depth is independent of offset. Therefore, the corrected imaged-depths from different offsets should be close to each other. Suppose that there are offsets h_1, h_2, …, h_m, and image locations x_1, x_2, …, x_K, then:

$$z_j^k + \delta Z^k = z_j^k + \sum_{i=1}^{n} g_{ij}^k\ \delta\lambda_i \quad \text{A.14}$$

where

$$z_j^k = z\left(x_k, h_j\right), \delta Z^k = \delta z\left(x_k, h_j\right), g_{ij}^k = g_i\left(x_k, h_j\right)$$

Supposing that the corrected imaged depths have the minimum variance, the solution of $\delta\widehat{\lambda}$ must satisfy the linear equation:

$$\left[\sum_{k=1}^{K} A^k\right]\delta\widehat{\lambda} = -\sum_{k=1}^{K} b^k \quad \text{A.15}$$

where the matrix A^k is equal to:

$$A^k \equiv \left[a_{il}^k\right]_{n\times n}$$

and the vector b^k is equal to:

$$b^k \equiv \left(b_1^k, b_2^k, ..., b_n^k\right)$$

where

$$a_{il}^k = \sum_{j=1}^{m}\left(g_{ij}^k - \underline{G_i^k}\right)\left(g_{lj}^k - \underline{G_l^k}\right),$$

$$b_i^k = \sum_{j=1}^{m}\left(g_{ij}^k - \underline{G_i^k}\right)\left(z_j^k - \underline{Z^k}\right),$$

$$G_i^k = \left(g_{i1}^k, g_{i2}^k, ..., g_{in}^k\right),$$

$Z^k = \left(z_1^k, z_2^k, ..., z_m^k\right)$.

The overline denotes the mean value over offset index.

If there is only one parameter (i.e., n = 1, which is the case implemented in Seismic Unix), then the eq. A.15 has the following explicit solution:

$$\delta\lambda = -\frac{\sum_{k=1}^{K}\sum_{j=1}^{m}\left(g_j^k - \underline{G^k}\right)\left(z_j^k - \underline{Z^k}\right)}{\sum_{k=1}^{K}\sum_{j=1}^{m}\left(g_j^k - \underline{G^k}\right)^2} \quad \text{A.16}$$

where

$g_j^k = g\left(x_k, h_j\right), G^k = \left(g_1^k, g_2^k, ..., g_m^k\right)$

It is clear that, if the corrected imaged depths are not close enough to each other, an iteration procedure is necessary to obtain more accurate parameters. Finally, it is important to underline that if too many parameters are considered, the solution will be underdetermined and unstable. Consequently, it is essential to characterise the velocity distribution by choosing appropriate parameter numbers.

Derivative function calculation

Let us consider the eikonal equation:

$$\left(\frac{\partial\tau}{\partial x}\right)^2 + \left(\frac{\partial\tau}{\partial z}\right)^2 = \frac{1}{v^2(x;\lambda)} \quad \text{A.17}$$

and its derivative with respect to λ. Its integral solution is:

$$\mu = \int_L \frac{\partial}{\partial\lambda}\left(\frac{1}{v^2(x;\lambda)}\right) dL \quad \text{A.18}$$

where

$$\mu = \frac{\partial\tau}{\partial\lambda} \quad \text{A.19}$$

and L is the raypath from the source (or receiver) to the image point x. From each source or receiver, μ can be determined from eq. A.18. Therefore, given an image point x and a specular source-receiver pair x_s and x_r, g can be calculated by using eq. A.6. Because there is no explicit formula to represent the specular source-receiver pair from the image point for a complex medium, the Kirchhoff integral can be used to calculate g by using the same technique used by Bleistein et al. (1987) to evaluate the angle of reflection in Kirchhoff's inversion.

Liu's approach consists in calculating two migration outputs which have the same phase but different amplitudes: the original amplitude and the original amplitude multiplied by the quantity g. Thus, the ratio of the amplitudes of these two outputs is equal to g at the specular source-receiver position according to the stationary-phase principle.

Seismic Unix codes

In the following, we report the list of the codes necessary to perform the PSDM and update the velocity by using the Liu approach.

DZDV - determine depth derivative with respect to the velocity parameter, *dz/dv*, by ratios of migrated data with the primary amplitude and those with the extra amplitude.
VELPERT - estimate velocity parameter perturbation from covariance of imaged depths in CIGs.
SURELAN - compute residual-moveout semblance r for CDP gathers based on *z(h)*z(h) = z(0)*z(0) + r*h*h* where *z* is depth and *h* offset.
RAYT2D - traveltime tables calculated by 2D paraxial ray tracing
SUKDMIG2D - Kirchhoff pre-stack depth migration of 2D data

References

Bleistein, N., Cohen, J., Hagin, F., 1987. Two and one-half dimensional Born inversion with an arbitrary reference. Geophysics 52, 26–36.

Cohen, J.K., Stockwell Jr., J.W., 2008. CWP/SU: Seismic Unix Release No. 41: an Open Source Software Package for Seismic Research and Processing. Center for Wave Phenomena, Colorado School of Mines.

Giustiniani, M., Accaino, F., Picotti, S., Tinivella, U., 2009. 3D seismic data for shallow aquifers characterisation. J. Appl. Geophys. 68 (3), 394–403.

Giustiniani, M., Tinivella, U., Nicolich, N., 2018. Crustal structure of central Sicily. Tectonophysics 722, 299–313.

Giustiniani, M., Tinivella, U., Nicolich, N., 2022. Imaging subsurface structures using wave equation datuming advanced seismic techniques. In: Bell, Rebecca, Iacopini, David, Vardy, Mark (Eds.), Interpreting Subsurface Seismic Data, vol. 2022. Elsevier, pp. 199–234. https://doi.org/10.1016/B978-0-12-818562-9.00004-2.

Guo, B., Schuster, G.T., 2017. Wave-equation migration velocity analysis using plane-wave common-image gathers. Geophysics 82, S327–S340.

He, B., Liu, Y., 2020. Wave-equation migration velocity analysis using Radon-domain common-image gathers. J. Geophys. Res. Solid Earth 125, e2019JB018938.

Jones, I., 2010. An Introduction to: Velocity Model Building. EAGE publications, 0.3997/9789073834958.

Jones, I.F., 2014. Estimating subsurface parameter fields for seismic migration: velocity model building. In: Grechka, V., Wapenaar, K. (Eds.), Encyclopedia of Exploration Geophysics. Society of Exploration Geophysicists. U1-1-U1-24.

Liu, Z., 1995. Migration Velocity Analysis. Doctoral Thesis. Center for Wave Phenomena Colorado School of Mines.

Liu, Z., Bleistein, N., 1995. Migration velocity analysis: theory and an iterative algorithm. Geophysics 60, 142e153.
Loreto, M.F., Tinivella, U., 2012. Gas hydrate versus geological features: The South Shetland case study. Mar. Petrol. Geol. 36 (1), 164–171.
Loreto, M.F., Tinivella, U., Accaino, F., Giustiniani, M., 2011. Gas hydrate reservoir characterization by geophysical data analysis (offshore Antarctic Peninsula). Energies 4, 39–56.
Loreto, M.F., Tinivella, U., Ranero, C.-R., 2007. Evidence for fluid circulation, overpressure and tectonic style along the Southern Chilean margin. Tectonophysics 429, 183–200.
Sain, K., Nara, D., 2023. Active Seismic Tomography: Theory and Applications. Wiley, ISBN 978-1-119-59486-4.
Tinivella, U., Loreto, M.F., Accaino, F., 2009. Regional versus Detailed Velocity Analysis to Quantify Hydrate and Free Gas in Marine Sediments: the South Shetland Margin Case Study, vol. 319. Geological Society Special Publication, pp. 103–119.
Vargas-Cordero, I., Tinivella, U., Accaino, F., Loreto, M.F., Fanucci, F., 2010a. Thermal state and concentration of gas hydrate and free gas of Coyhaique, Chilean Margin (44°30′ S). Mar. Petrol. Geol. 27 (5), 1148–1156, 2010.
Vargas-Cordero, I., Tinivella, U., Accaino, F., Loreto, M.F., Fanucci, F., Reichert, C., 2010b. Analyses of bottom simulating reflections offshore Arauco and Coyhaique (Chile). Geo Mar. Lett. 30 (3–4), 271–281.
Vargas-Cordero, I.C., Tinivella, U., Villar-Muñoz, L., Giustiniani, M., 2016. Gas hydrate and free gas estimation from seismic analysis offshore Chiloé island (Chile). Andean Geol. 43 (3), 263–274.
Vargas-Cordero, I.C., Tinivella, U., Villar-Muñoz, L., 2017. Gas hydrate and free gas concentrations in two sites inside the Chilean margin (Itata and Valdivia offshores). Energies 10 (12). Article number 2154.
Vargas-Cordero, I.C., Tinivella, U., Villar-Muñoz, L., Bento, J.P., 2018. High gas hydrate and free gas concentrations: an explanation for seeps offshore south mocha island. Energies 11 (11), 3062.
Vargas-Cordero, I.C., Villar-Muñoz, L., Tinivella, U., Giustiniani, M., Bangs, N., Bento, J. P., Contreras-Reyes, E., 2021. Gas origin linked to paleo BSR. Sci. Rep. 11 (1) https://doi.org/10.1038/s41598-021-03371-z. Article number 23960.
Villar-Muñoz, L., Bento, J.P., Klaeschen, D., Tinivella, U., Vargas-Cordero, I., Behrmann, J., 2018. A first estimation of gas hydrates offshore Patagonia (Chile). Mar. Petrol. Geol. 96, 232–239.
Villar-Muñoz, Vargas-Cordero, I., L, Bento, J.P., Tinivella, U., Fernandoy, F., Giustiniani, M., Behrmann, J., Calderón-Díaz, S., 2019. Gas hydrate estimate in an area of deformation and high heat flow at the Chile triple junction. Geosciences 9 (11). Article number 28.
Xiang, K., Landa, E., 2017. Comparisons between common-image gathers and common midpoint gathers for AVO analysis: a case study on gas reservoir. In: SEG Technical Program Expanded Abstracts, pp. 697–701.
Yilmaz, O., 2001. Seismic Data Analysis: Processing, Inversion and Interpretation of Seismic Data, second ed. Society of Exploration Geophysicists, Tulsa, Oklahoma, p. 2027.